

Towards the Development of Tactile Sensors for Determination of Static Friction Coefficient to Surfaces

M. Scharff, M. Darnieder, J. Steigenberger and C. Behn

Abstract Natural vibrissae fulfill a lot of functions. Next to object distance detection and object shape recognition, the surface texture can be determined. Inspired by the natural process of surface texture detection, the goal is to adapt this feature by technical concepts. Modeling the vibrissa as an Euler–Bernoulli bending beam with a quasi-statically moving support and the vibrissa–surface contact with respect to Coulomb’s Law of Friction, a first approach was formed by the group of Behn and Steigenberger. Due to the motion of the support (pushing the vibrissa) and the surface contact, the vibrissa gets deformed. Firstly, the beam tip is sticking to the surface. The acting friction force prevents a movement of the beam tip until the maximal stiction is reached. The displacement of the support corresponds to changes in the acting forces and moments. Out of these changes the coefficient of static friction can be determined. The analytical results of Steigenberger and Behn are verified and validated by numerical simulations and an experiment.

Keywords Surface detection · Vibrissae · Friction · Mechanical contact · Beam

1 Introduction

Rodents scan the surrounding environment with different sensory organs. Besides of eyes and ears they use tactile hairs, named *vibrissae*. Vibrissae exist, e.g., at the paws (*carpal vibrissae*) and in the snout region (*mystacial vibrissae*) (Helbig et al. 2014).

In order to simplify the natural sophisticated example of a vibrissa and related periphery from a mechanical point of view, usually the following assumptions are

M. Scharff (✉) · M. Darnieder · C. Behn
Technical Mechanics Group, Department of Mechanical Engineering,
Technische Universität Ilmenau, Ilmenau, Germany
e-mail: moritz.scharff@tu-ilmenau.de

J. Steigenberger
Faculty of Mathematics and Natural Sciences, Institute of Mathematics,
Technische Universität Ilmenau, Ilmenau, Germany

done. Each vibrissa is held by a viscoelastic support, which is maybe controllable. A vibrissa has a tapered shape, whereby the diameter of the cross-section is decreasing from base to tip. The diameter of the cross section is much smaller than the length of a vibrissa. Along their whole length, vibrissae are naturally pre-curved (stress free).

From the inside to the outside of the vibrissa there are three layers made out of different materials. The thickness of each layer changes along the length of the vibrissa (Voges et al. 2012).

The complex morphology offers a wide functionality of the vibrissa. They are used for distance evaluation, object shape recognition and surface texture detection (Carl et al. 2011).

2 State of the Art

The natural process of surface texture detection is not completely understood yet. It is observed that, e.g., a rat follows a special control strategy. If the vibrissae get into contact with a surface the rat will position its head in the way that a maximum quantity of vibrissae are in touch while they are minimally deformed, (Mitchinson et al. 2007; Grant et al. 2009). Out of this position, the rat starts whisking. Three to five whisk-cycles are needed to collect the information (Carvell and Simons 1990).

For the procedure of the transduction of the mechanical stimuli into a signal and finally into a property of the surface, there are several hypotheses. The authors of Moore and Andermann (2005) formulate the *resonance hypothesis*. They assume that there is a relation between the frequency of the vibrissa and the surface roughness inducing vibration. Alike to the resonance hypothesis are the works (Arabzadeh et al. 2005; Hipp et al. 2006). They are based on the recording of pattern of vibrissa motion events under different velocities, which represent the surface texture. The authors of Wolfe et al. (2008) analyze another concept. Based on the *Stick-Slip-Effect*, the frequency of stick-slip events and the distance between the sticking periods are related to the surface roughness. A high frequency of stick-slip events and a large distance between the sticking periods indicate a high roughness of the surface.

Under aspects of applied mechanics, these three theories need further analytical treatment. A first approach that gives a complete, analytical description is done in Steigenberger et al. (2015), which forms the basis of this work.

3 Aim and Scope

The surface texture detection is a critical point in literature. Known hypotheses were studied and proofed empirically, but there is still a lack of knowledge as well. Adding new aspects to the present works, a discussion of the mechanical theory

behind the hypotheses—described above—has to be done. Using the theory of Steigenberger et al. (2015), a *first* approach to a sensor concept is discussed, where we try to determine the static coefficient of friction μ_0 at first.

4 Modeling

Using the *Euler–Bernoulli beam theory* with respect to large deflections, the single vibrissa is modeled as a straight beam with a cylindrical cross-section. In a very first step, the clamping replaces the viscoelastic support. The resulting frictional force acts at the tip of the beam. The load acts only in the x-y-plane and is considering *Coulomb’s Law of Friction* with respect to stiction. With a view to a technical sensor, the beam consists of *Hooke material*.

To find generally valid statements about the discussed theory, a nondimensionalization takes place with respect to the following basic parameters:

$$\text{units: } [\text{length}] = L; [\text{force}] = EI_z L^{-2}; [\text{moment}] = EI_z L^{-1}$$

whereby L is the length, E is the Young’s Modulus, I_z is the second moment of area. For example: if we consider a steel beam with the basic parameters $E = 2.10 \cdot 10^5$ MPa, $I_z = 250$ mm⁴, $L = 100$ mm, than a value $f = 1.33$ during dimensionless calculation results in the following real force:

$$F = f \cdot [\text{force}] = f \cdot \frac{EI_z}{L^2} = 7000 \text{ N}$$

The system also gets normalized by assuming the arc length coordinate s in the interval:

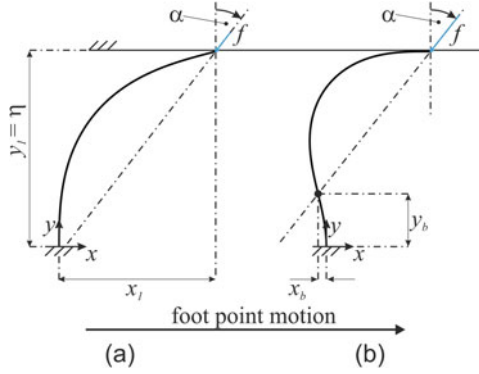
$$s \in [0, 1]$$

The idea behind the model out of Steigenberger et al. (2015) is sketched in Fig. 1. The beam is deformed and the tip is touching a surface at the point (x_1, y_1) , see Fig. 1a. The parameter η describes the distance between the clamping and the assumed horizontal surface. Initializing a displacement (quasi-static) of the foot point (clamping) in x -direction, the beam gets further deformed. If the static friction coefficient μ_0 (respectively the angle of static friction α_0) of the surface combination is large enough, there is an *inflection point*, see Fig. 1b. An inflection point marks a sign change of the curvature of the deformed shape of the beam. The sign change is located at the point (x_b, y_b) .

The dash-dotted line means the following:

- Passing right to the clamping there exist no inflection point;
- Passing through the clamping means a zero clamping moment;

Fig. 1 Relations and definitions of the system states, adapted from Steigenberger et al. (2015)



- Passing left to the clamping results in an inflection point, whereby we have a zero bending moment at the intersection point to the beam.

To study the relations between the present μ_0 and the resulting reaction forces and moments in the clamping, the equilibrium state conditions are formulated in the following way:

$$\mathbf{M}_{bz}(s) = \mathbf{r} \times \mathbf{f} = f (\cos(\alpha) (x(s) - x_1) + \sin(\alpha) (y(s) - y_1)) \vec{e}_z \quad (1)$$

According to the parametric representation the system of equations yields to:

$$\left. \begin{aligned} x'(s) &= \cos(\varphi(s)) \\ y'(s) &= \sin(\varphi(s)) \\ \varphi'(s) &= f (\cos(\alpha) (x(s) - x_1) + \sin(\alpha) (y(s) - y_1)) \end{aligned} \right\} \quad (2)$$

with boundary conditions:

$$\left. \begin{aligned} x(0) &= 0 & ; & & x(1) &= x_1 \\ y(0) &= 0 & ; & & y(1) &= y_1 \\ \varphi(0) &= \frac{\pi}{2} & ; & & \varphi(1) &= \phi_1 \end{aligned} \right\} \quad (3)$$

The function φ is the slope of the deformed shape of the beam. The system of Eq. (2) and the corresponding boundary conditions (3) form a free boundary value problem (BVP) with two unknown quantities.

Remark Using Matlab R2016a, the system of Eqs. (2) and (3) is solved in applying a *Shooting-Method*: starting from a guess for the unknown quantities, the values of the unknown quantities are optimized by performing the 2D-optimization function *fminsearch()*. In every step of the optimization, the system of equations is solved by the *Runge-Kutta-Method of 4th order*.

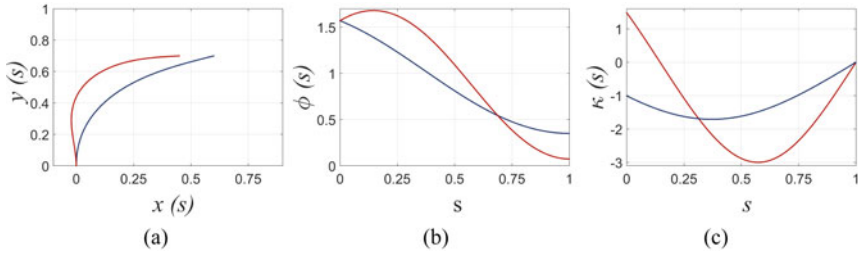


Fig. 2 Relations and definitions of the two system states, adapted from Steigenberger et al. (2015). **a** The deformed shapes of both states in dependence on cartesian coordinates. The related slope and curvature trends are plotted in **(b)** and **(c)**

As already mentioned, the inflection point occurs when there is a sign change in the curvature, see Fig. 2. The blue line corresponds to a solution without an inflection point and the red line to one with one.

The trends of the functions for the curvature show the assumed behavior. There is no sign change of $\kappa(s)$ for the state without a inflection point. On the contrary, a sign change of $\kappa(s)$, from positive to negative, belongs to a state with an inflection point.

5 Simulation and Experiment

The system of Eq. (2) with its boundary conditions (3) is solved for a sequence of $x_1 = -0.2$ (0.05) 0.6 and a fixed $\eta = 0.75$, see Fig. 3.

Remark From now on, the representation of the results reverses reality: fixed support and moving contact point (tip of the beam).

There are two shapes without and fifteen with an inflection point. The appearance of an inflection point corresponds to smaller x_1 . From the left to right, α is negative and decreasing until the first shape without inflection point occurs, see Fig. 4a. For this shape α takes larger values. This trend also goes on for the last shape. In this configuration α becomes positive. That means the complete force starts pulling the beam, with view to real scenario this case is out of interest.

Figure 4b indicates that there are two solutions for the same φ_1 . So, φ_1 cannot be used to identify any surface properties because the result is not unique. Figure 5 shows the deformed shapes for a sequence of $y_1 = 0.4$ (0.025) 0.875 and a fixed $x_1 = 0.45$. From top to bottom, there are three solutions without and seventeen with an inflection point. At $y_1 = 0.875$, α and the acting forces are positive again, see Fig. 6a, c. This is equal to the previous finding; in this configuration the beam gets pulled.

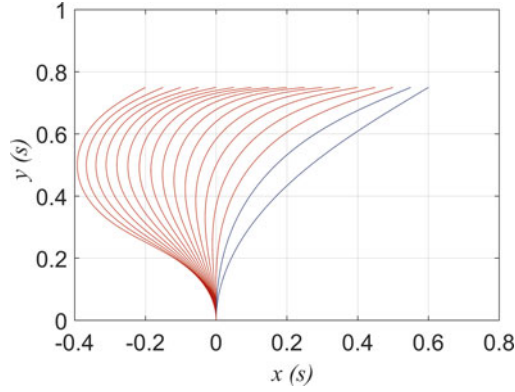


Fig. 3 In contrary to the two *blue* shapes, the fifteen *red* ones show an inflection point. The inflection point occurs in dependence on the tip coordinate x_1

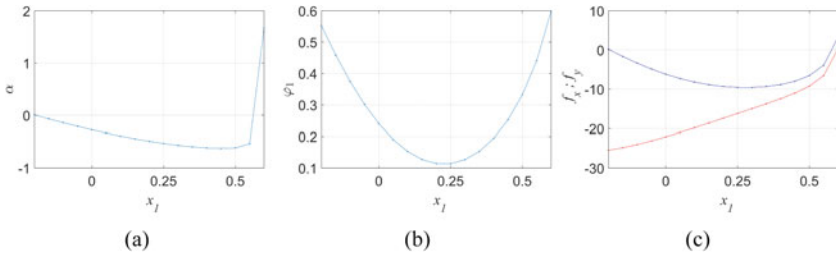
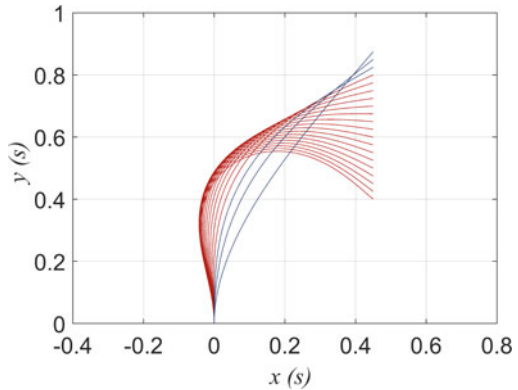


Fig. 4 **a** The static friction angle α versus x_1 ; **b** Relation between the slope in the beam tip φ_1 and x_1 ; **c** The trend of the acting forces f_x (*blue*) and f_y (*red*) in dependence on x_1

Fig. 5 For a sequence of y_1 and a fixed x_1 twenty solutions are calculated. There are three solutions without and seventeen ones with inflection point. There are negative values for φ_1 when y_1 is small



There are solutions that belong to negative values of φ_1 . These solutions show values for $y(s) \geq y_1$. In reality, this is impossible. If $\eta \leq y(s)$, the beam has to penetrate the surface. These solutions are correctly computed but should be omitted, because $\varphi_1 < 0$.

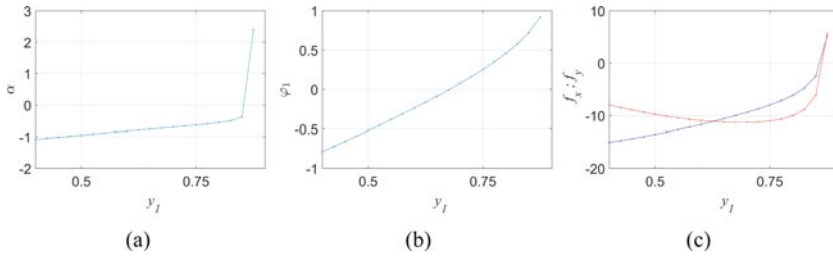


Fig. 6 **a** The static friction angle α versus y_1 ; **b** Relation between the slope in the beam tip φ_1 and y_1 ; **c** The trend of the acting forces f_x (blue) and f_y (red) in dependence on y_1

While y_1 is increasing, so φ_1 does. The slope $\varphi_1 = \frac{\pi}{2}$ when $y_1 = L$ and $x_1 = 0$. Combing the findings of the Figs. 3, 4, 5 and 6, it follows that the appearance of an inflection point depends on, e.g., the coordinate of the beam tip (respectively the value of α). This means, for every η , there is a μ that belongs to a shape with an inflection point. The relation is shown in Fig. 7. For each value of a sequence of $\eta = 0.05$ (0.05) 0.85 solutions for a sequence of $x_1 = -0.02$ (0.01) 0.6 are computed. Out of these solutions for each value of η , the last one without and the first one with an inflection point are collected. The exact limit for the appearance of an inflection point is located between these two solutions. Figure 7 indicates that for large values of η smaller values of μ are required to get an inflection point.

To validate the numerical simulations an experiment is performed. Using a stepping motor as a drive and a steel band as a vibrissa/sensor, the deformations of the structure are analyzed while it is touching a surface. Using an image tracking system, the collected information are compared to the simulation, see Fig. 8. There

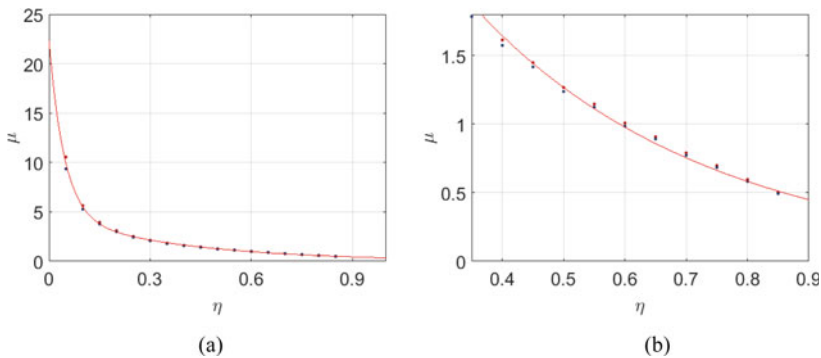


Fig. 7 Trend of the appearance of an inflection point. The blue points are the last solution without and the red points the first solution with inflection point. The red, solid line illustrates a fitted exponential function due to the mean values of the point pairs. The figure part (b) shows a zoom on the area of interest

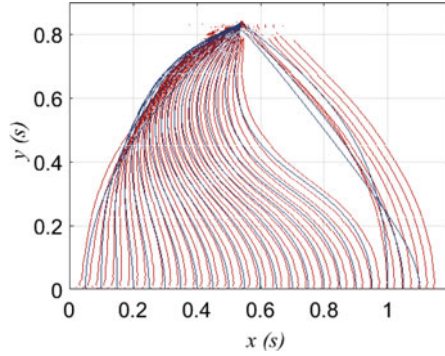


Fig. 8 The simulated shapes (*blue*) are compared to the shapes out of measured data (*red*)

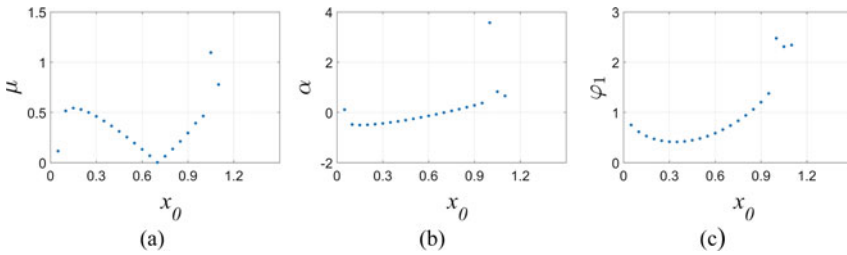


Fig. 9 **a** Static friction coefficient μ versus foot point coordinate x_0 . **b** In addition to **(a)**, instead of μ , α is plotted. **c** Trend of φ_1 over x_0

is a good matching of the simulation and the experimental data. The initial shapes show a larger deviation to each other than the following ones. This is caused by the effect that the real structure is loaded by unknown forces while it is located in the initial position. Around $x_1 \approx 1$ the sensor *jumps* into the next equilibrium state. Both the simulation and the experiment show this *snap*. The shapes after the snap show a larger deviation between simulation and experiment than the ones before. In the experiment, the sensor tip moves while the structure is turning over. On the contrary, for the simulation, the tip of the beam is fixed to one point.

This dynamic effect maybe caused by the stepping motor because for every step there is an impulse. The snap occurs for high values of μ , see Fig. 9a. If the snap occurs, the tip of the sensor is not pushed anymore, it is pulled. In this case, the mentioned sensor concept will fail.

In this experiment, the snap probably occurs when $\varphi_1 = \frac{\pi}{2}$, see Figs. 8 and 9c. The trend of φ_1 in Fig. 9c indicates a similar behavior than the one in Fig. 4b. In both cases there is a parabola-like trend.

6 Conclusions

The analytical work in Steigenberger et al. (2015) was verified by numerical simulations and validated by an experiment. It is possible to determine the coefficient of static friction μ_0 out of the deformation of the sensor.

$$\tan(\alpha) = \frac{F_T}{F_N} = \mu \leq \mu_0 = \tan(\alpha_0) \quad (4)$$

Measuring the reaction forces to the tangential and normal force F_T , F_N at the sensor support, μ can be determined by using (4). In the course of further moving of the support μ increases until μ_0 is reached. For $\mu_0 \leq \mu$ the beam tip snaps off. So, the last measured values of the reaction forces before the snap off corresponds to μ_0 .

The simulations show, if the distance η between vibrissa base and contact surface is small, there are no solutions of practical interest. This leads immediately to the claim in formulating a stringent restriction of the deformations ($y(s) \leq \eta$, $\forall s \in (0, 1)$). Both, simulation and experiment show that inflection points and a snap occur.

While the snap leads to a fail of the sensor, the inflection point can be used as an input signal for the sensor. When the inflection point occurs, the curvature $\kappa(0)$ at the vibrissa base respectively the bending moment $M_{b_z}(0)$ are equal to zero. This configuration can be easily detected by a torque sensor. Out of the information that there is an inflection point the belonging μ_0 can be determined. The inflection point configuration for any surface can be found by controlling η and sweeping the sensor tip over the surface until $M_{b_z}(0) = 0$. Then the value of μ_0 follows out of the relation of Fig. 7 in combination with the known η .

This work is restricted due to various simplifications and is continued under various aspects. The influence of the mentioned real morphology of a vibrissa for a technical sensor has to be analyzed. To study a more realistic scenario the boundary conditions have to be modified, in the way that they represent a contact plane and not only a contact point. Inspired by the findings out of literature, the analytical considerations are enhanced to dynamics, to consider effects like stick-slip. In the course of this, the used mechanical model will be optimized under aspects of tribology.

References

- Arabzadeh E, Zorzin E, Diamond ME (2005) Neuronal encoding of texture in the whisker sensory pathway. *PLoS Biol* 3(1):1–11
- Carl K, Hild W, Mämpel J, Schilling C, Uhlig R, Witte H (2011) Characterization of statical properties of rat's whisker system. *IEEE Sens J* 12(2):340–349
- Carvell GE, Simons DJ (1990) Biometric analyses of vibrissal tactile discrimination in the rat. *J Neurosci* 10(8):2638–2648

- Grant R, Mitchinson B, Fox C, Prescott T (2009) Active touch sensing in the rat: anticipatory and regulatory control of whisker movements during surface exploration. *J Neurophysiol* 101(2):862–874
- Helbig T, Voges D, Niederschuh S, Schmidt M, Witte H (2014) Characterizing the substrate contact of carpal vibrissae of rats during locomotion. In: Proceedings of the 3th international conference, living machines, Milan, Italy, 30 July–1 Aug 2014, 3 pages
- Hipp JE, Arabzadeh E, Zorzin E, Conradt J, Kayser C, Diamond ME, König P (2006) Texture signals in whisker vibrations. *J Neurophysiol* 95(3):1792–1799
- Mitchinson B, Martin C, Grant R, Prescott T (2007) Feedback control in active sensing: rat exploratory whisking is modulated by environmental contact. *Proc R Soc B* 274:1035–1041
- Moore C, Andermann M (2005) The vibrissa resonance hypothesis. In: Somatosensory plasticity. CRC Press, Boca Raton, pp 21–60
- Steigenberger J, Behn C, Will C (2015) Mathematical model of vibrissae for surface texture detection. Preprint No. M 13/03. Technische Universität Ilmenau. 16 pages
- Voges D, Carl K, Klauer G, Uhlig R, Schilling C, Behn C, Witte H (2012) Structural characterization of the whisker system. *IEEE Sens J* 12(2):332–339
- Wolfe J, Hill DN, Pahlavan S, Drew PJ, Kleinfeld D, Feldman DE (2008) Texture coding in the rat whisker system: slip-stick versus differential resonance. *PLoS Biol* 6(8):1–17